Turk J Elec Engin, VOL.10, NO.2 2002, © TÜBİTAK

Iterative Solution of Field Problems with a Varying Physical Parameter

Anton G. TIJHUIS, Martijn C. van BEURDEN
Faculty of Electrical Engineering, Eindhoven University of Technology
P.O. Box 513,5600 MB Eindhoven, the NETHERLANDS
e-mail: A.G.Tijhuis@tue.nl
A. Peter M. ZWAMBORN
TNO Physics and Electronics Laboratory,
P.O. Box 96864,2509 JG 's-Gravenhage, the NETHERLANDS
Faculty of Electrical Engineering, Eindhoven University of Technology
P.O. Box 513,5600 MB Eindhoven, the NETHERLANDS

Abstract

In this paper, linear field problems with a varying physical parameter are solved with the conjugate-gradient FFT method and a dedicated extrapolation procedure for generating the initial estimate. The scheme is formulated and illustrated for two simple example problems. The importance of the choice of the stop criterion and the step size are demonstrated for the case of a straight thin-wire segment. A brief summary is given of the applications that have appeared in the open literature until now, and actual three-dimensional scattering problems for a rectangular conducting plate and an inhomogeneous, dispersive dielectric body are discussed. Finally, the case where the medium surrounding the object of interest is no longer homogeneous is addressed for two representative examples: wire antennas over a layered half space and an inhomogeneous dielectric cylinder in a water-filled container.

Key Words: *Field computations, iterative techniques, initial estimate, wire and patch antennas, dielectric object, embedding.*

1. Introduction

In modern society different trends are recognized in the usage of the available electromagnetic spectrum. One can think of wireless communication or transport of (digital) information. The density of such applications is increasing rapidly. Obtaining electromagnetic compatibility and/or reducing electromagnetic interference sometimes seems to be an impossible task. Another trend is found in electromagnetic inverse scattering and profiling. For example, this development is used in the detection and classification of land mines and other unexploded ordnance. Regarding electromagnetic inversion, one can also think of medical applications such as tomography or the detection of defects in metallic heart valves. Finally, we would like to mention the problem of electromagnetic coupling into humans in the area of clinical hyperthermia or non-ionizing radiation hazards analysis. In these applications, a rigorous electromagnetic analysis is indispensable.

The focus of this paper is found in computational tools in the field of electromagnetic analysis and design. One can identify the roadmap "going from engineering electromagnetics to electromagnetic

engineering". One of the extensively used and most versatile methods is the integral equation technique. It takes into account that the irradiated object is present in free space and that it manifests itself through the presence of secondary sources or contrast sources. Integral equations can be solved by the Method of Moments (MoM) [1], in which the unknown field function is expanded in a sequence of expansion functions. Subsequently, both sides of the integral equation are multiplied by a sequence of testing functions, and the results are integrated over the object domain. This leads to a system of linear algebraic equations.

To solve this system, one can use direct discrete numerical solution methods, such as Gaussian Elimination (GE) or Singular Value Decomposition (SVD), or suitable iterative techniques such as a conjugate-gradient method (CG). An overview of numerical solution methods for linear systems of equations can be found in [2]. In electromagnetic scattering and coupling problems, integral equations are often solved by using a Fast Fourier Transform (FFT) to compute the spatial convolution of the integral operator and a conjugate-gradient iterative scheme. This so-called CGFFT method has been used successfully for many electromagnetic scattering and coupling problems [3-9].

In analysis or design procedures, the engineer has the freedom to change one or more parameters to obtain an optimal design with respect to performance and costs. This means that he or she will need to consider the determination of electromagnetic fields for a (large) number of values of a physical parameter. In this paper we present a strong approach for this type of problem, which utilizes the iterative schemes mentioned above. We restrict ourselves to the case where the linear system originates from one or more integral equations. We apply an iterative procedure based on the minimization of an integrated squared error, and start this procedure from an initial estimate that is a linear combination of the last few "final" results. When the coefficients in this extrapolation are determined by minimizing the integrated squared error for the actual value of the parameter, the built-in orthogonality in this type of scheme ensures that only a few iteration steps are required to obtain the solution.

The outline of the paper is as follows. In Section 2, the method of solution is discussed. Special attention is given to the iterative procedure and the implementation of a relevant initial estimate based on the previous solutions. In Section 3, a simple example is given to clarify the success of the present approach. In Section 4, the behavior of our approach is illustrated for the simple case of a straight thin wire segment. In Section 5, a short review of already obtained results is given, and explicit examples are discussed in Section 6 and 7. Finally, Section 8 presents the conclusions.

2. Method of Solution

In the computational modeling of electromagnetic fields for practical applications, typically a large system of linear equations must be solved. This system originates from spatially discretizing MaxwelI's differential equations (in "finite" or "local" techniques) or equivalent integral equations (in "global" techniques). In formal notation, such a system can be written as

$$L(p)\,u(p) = f(p)\,, \tag{1}$$

where $L(p)$ = a linear operator, $u(p)$ = the unknown field, $f(p)$ = the forcing function, p = a physical parameter.

The operator $L(p)$ originates from discretizing its counterpart in the continuous equation, $u(p)$ is a discretized field and $f(p)$ corresponds to an impressed source or an incident field. We are interested in the

situation where this problem must be solved for a large number of sampled values of the parameter p, e.g., $p = p_o + m\Delta p$, with $m = 0,1, ..., M$.

2.1. Iterative procedure

In this subsection, we consider the iterative procedure that is used to solve the system of equations (1). We summarize the classical description of Van den Berg [3,4], but restrict ourselves to the case where (1) is a discretized equation. We do account for the case where (1) is an overdetermined system.

First, we introduce an inner product. Let g and h be two vectors in data space, i.e., the space in which the vectors Lu and f are defined. Then, we define the inner product as

$$\langle g|h\rangle = \sum_j g_j^* h_j, \tag{2}$$

where g_j and h_j denote the components of g and h, and where the asterisk denotes complex conjugation. Further, we define a norm according to

$$\|g\|^2 = \langle g|g\rangle. \tag{3}$$

The basic idea behind the iterative procedure is to construct a sequence of vectors $\{u^{(n)}|n = 0, 1, 2, ...\}$ such that the norm of the residual in (1), i.e.,

$$ERR^{(n)} = \left\langle r^{(n)}|r^{(n)}\right\rangle^{1/2}, \quad with \quad r^{(n)} = Lu^{(n)} - f, \tag{4}$$

decreases with increasing n. At each step of the iterative procedure, we write

$$u^{(n)} = u^{(n-1)} + u_{cor}^{(n)}, \tag{5}$$

where $u_{cor}^{(n)}$ is a suitably constructed correction vector. We start the procedure with an initial guess $u^{(0)}$ with corresponding residual $r^{(0)}$, and a suitably chosen variational vector $\varphi^{(1)}$. Let

$$u_{cor}^{(1)} = \alpha^{(1)}\varphi^{(1)}. \tag{6}$$

We now determine the scalar $\alpha^{(1)}$ such that $\left\langle r^{(1)}|r^{(1)}\right\rangle$ is minimized. This leads to

$$\alpha^{(1)} = \frac{-\left\langle L\varphi^{(1)}|r^{(0)}\right\rangle}{\left\|L\varphi^{(1)}\right\|^2}. \tag{7}$$

In subsequent steps, we let

$$u_{cor}^{(n)} = \alpha^{(n)}\hat{u}_{cor}^{(n)} \text{ with } \hat{u}_{cor}^{(n)} = \varphi^{(n)} + \beta^{(n)}\hat{u}_{cor}^{(n-1)}, \tag{8}$$

for n = 2,3, ... In (8), $\varphi^{(n)}$ is again a suitably chosen variational vector. It now follows $\langle r^{(n)}|r^{(n)}\rangle$ is minimized when

$$\alpha^{(n)} = \frac{-\langle L\varphi^{(n)}|r^{(n-1)}\rangle}{\left\|L\hat{u}_{cor}^{(n)}\right\|^2}, \tag{9}$$

and

$$\beta^{(n)} = \frac{\left\langle L\hat{u}_{cor}^{(n-1)}|L\varphi^{(n)}\right\rangle}{\left\|L\hat{u}_{cor}^{(n-1)}\right\|^2}. \tag{10}$$

With equations (5)-(10) the iterative scheme based on error minimization has been defined.

A geometrical interpretation is that, in each iteration step, the component of the residual $r^{(n-1)}$ in the subspace spanned by the basis vectors $L\varphi^{(n)}$ and $Lu_{cor}^{(n-1)}$ is removed by the correction $\alpha^{(n)}\hat{u}_{cor}^{(n)}$. This can also be seen from the fact that

$$\left\langle r^{(n)}|L\varphi^{(n)}\right\rangle = 0 \quad for \quad n \geq 1, \quad and \quad \left\langle r^{(n)}|Lu_{cor}^{(n-1)}\right\rangle = 0 \qquad for \quad n \geq 2. \tag{11}$$

For a general choice of the expansion vectors $\left\{\varphi^{(n)}\right\}$, the successive basis vectors $\left\{Lu_{cor}^{(n)}\right\}$ are not orthogonal. Therefore, the iterative procedure formulated above cannot be interpreted as a full projection scheme.

2.2. Choice of expansion vectors

In principle, the iterative procedure outlined above works for any choice of the expansion vectors $\left\{\varphi^{(n)}\right\}$. The error is reduced as long as the coefficient $\alpha^{(n)}$ differs from zero, i.e., when

$$\left\langle L\varphi^{(n)}|r^{(n-1)}\right\rangle \neq 0. \tag{12}$$

The condition (12) is known as the *improvement condition*.

In the conjugate-gradient method, the expansion vectors are generated from the residuals:

$$\varphi^{(n)}(p_m) = L^{\wedge}(p_m)\, r^{(n-1)}(p_m), \tag{13}$$

where $L^{\wedge}$ is the adjoint operator corresponding to L. This choice offers the advantage that (12) is inherently satisfied. For this specific choice of expansion vectors, it can be shown that

$$\left\langle Lu_{cor}^{(n)}|L\varphi^{(j)}\right\rangle = 0 \quad and \quad \left\langle r^{(n)}|L\varphi^{(k)}\right\rangle = 0, \tag{14}$$

for $j = 0,1, ..., n\text{-}1$, and $k = 0,1, ..., n$, respectively. Now, any correction vector $u_{cor}^{(n)}$ is inherently a linear combination of the expansion vectors $\left\{\varphi^{(n)}\right\}$. Therefore, we may interpret the conjugate-gradient method as a successive projection of the residual $r^{(0)}$ on the orthogonalized basis vectors $\left\{L\varphi^{(n)}\right\}$.

In the remainder of this paper, we will restrict ourselves to this choice of expansion vectors. Further, we will attempt to organize the space discretization such that the convolution structure of the continuos equation is preserved. In that case, the matrix-vector products in (4) and (13) can be evaluated by FFT operations, which considerably improves the speed of the so-called CGFFT algorithm [3-9].

2.3. Initial estimate

In many applications of the conjugate-gradient method, a simple initial estimate is used. Typically, the scheme is started from $u^{(0)} = 0$. Depending on the nature of the problem at hand, we can also start from an incident field or from the Kirchhoff approximation to an unknown surface current.

Our choice of the initial estimate is inspired by the fact that $u(p)$ depends in a well-behaved manner on the parameter p. Therefore, it should be possible to extrapolate, by choosing

$$u^{(0)}(p_m) = \sum_{k=1}^{K} \gamma_k u(p_{m-k}). \tag{15}$$

The interpretation of the CG scheme given above suggested that the $\{\gamma_n | k = 1, ..., K\}$ should be found by minimizing the squared error

$$\left\langle L(p_m)\, u^{(0)}(p_m) - f(p_m) \,|\, L(p_m)\, u^{(0)}(p_m) - f(p_m) \right\rangle. \tag{16}$$

Because of the built-in orthogonality of the CG method, we are then certain that this procedure must start its search for components of $f(p_m)$ outside the space spanned by the "previous" functions $\langle Lu(p_{m-k}) \,|\, k = 1, ..., K\rangle$.

The coefficients γ_k that minimize the squared error (16) can be found from the system of linear equations

$$\sum_{k'=1}^{K} \langle L(p_m)\, u(p_{m-k}) \,|\, L(p_m)\, u(p_{m-k'})\rangle \gamma_{k'} = \langle L(p_m)\, u(p_{m-k}) \,|\, f(p_m)\rangle, \tag{17}$$

with $k = 1, ..., K$. Typically, we choose $K = 2$ (linear extrapolation) or $K = 3$ (quadratic extrapolation). For larger values of K, the basis vectors $L(p_m)\, u(p_{m-n})$ with $n = 1,..., K$ become almost linearly dependent, and therefore the coefficients $\{\gamma_k\}$ can no longer be resolved from (17).

3. A Simple Example

The authors are presently not aware of an exact analysis that provides an indication of the success of the extrapolation procedure outlined in Section 2.3. However, extensive numerical experimentation for a range

of problems has at least given an indication what is going on, and how computational parameters like step size and desired accuracy should be chosen.

In the present section, we will try to explain the efficiency of the CG-extrapolation procedure. To illustrate this, we consider the simple system of three linear equations

$$\begin{bmatrix} 1 & 0 & 0 \\ 0 & 1 & 0 \\ 0 & 0 & 2 \end{bmatrix} \begin{bmatrix} u_1 \\ u_2 \\ u_3 \end{bmatrix} = \begin{bmatrix} 1 \\ 1 \\ 2\Delta \end{bmatrix}, \tag{18}$$

which has the solution $u = [1, 1, \Delta]^T$. The 3×3 matrix in the left-hand side is representative of a well-conditioned, discretized integral equation. Since this integral equation is supposed to originate from a passive, linear physical problem, all eigenvalues will have the same order of magnitude. The idealizatian is that the corresponding eigenvectors are supposed to be orthogonal with respect to the inner product (2). The real-valued parameter $\Delta << 1$ in the right-hand side represents the effect of a step Δp in the physical parameter p. We consider the situation where only u_1 and u_2 correspond to modes that were excited for the previous value of p. For the initial estimate we take $u^{(0)} = [1 + \delta, 1 + \delta, 0]^T$, where δ may be envisaged as the extrapolation error. For convenience, we assume that δ is real-valued as well.

Carrying out the first iteration step as described in Section 2.1 then yields for the first correction vector:

$$u_{cor}^{(1)} = \frac{\delta^2 + 8\Delta^2}{\delta^2 + 32\Delta^2} \begin{bmatrix} -\delta \\ -\delta \\ 4\Delta \end{bmatrix}. \tag{19}$$

From (19), we observe that the first iteration step only leads to an effective correction of the error $u - u^{(0)} = [-\delta, -\delta, \Delta]$ when $|\delta| << |\Delta|$. Otherwise, we need to carry out all three iterations to obtain convergence.

In practice, the system of equations (1) is not always well conditioned. One possible cause is that the space discretization leading to such a system introduces spurious eigenvectors with a small eigenvalue. A second possibility is that the system is near resonance, and thus has a physical eigenmode with a small eigenvalue. In both cases, the requirements on the extrapolation error are even more severe. To illustrate this effect, we modify the system of equations (18) into

$$\begin{bmatrix} 1 & 0 & 0 \\ 0 & 1 & 0 \\ 0 & 0 & \Delta \end{bmatrix} \begin{bmatrix} u_1 \\ u_2 \\ u_3 \end{bmatrix} = \begin{bmatrix} 1 \\ 1 \\ \Delta \end{bmatrix}, \tag{20}$$

which has the solution $u = [1, 1, 1]^T$. We start from the same initial $u^{(0)} = [1 + \delta, 1 + \delta, 0]^T$, which means that we have a 100% error in the direction of the eigenvector corresponding to the small eigenvalue. Now, the first correction is found as

$$u_{cor}^{(1)} = \frac{2\delta^2 + \Delta^4}{2\delta^2 + \Delta^6} \begin{bmatrix} -\delta \\ -\delta \\ \Delta^2 \end{bmatrix}, \tag{21}$$

while the actual error at the start of the iteration scheme is $u - u^{(0)} = [-\delta, -\delta, 1]$. This means that we now have an almost complete correction in the first step only if $|\delta| << |\Delta|^3$.

In the actual implementation, we organize the discretization such that the dimension of the linear system (1) does not change, and that the elements of the system matrix $L(p)$ and the components of the vector $f(p)$ depend continuously on the physical parameter p. In that case, the changes represented by Δ in the above examples are proportional to the step Δp. The error in the initial estimate is represented by the small parameter δ. This means that in the realistic case represented by the second model even quadratic extrapolation with fixed coefficients, which leads to an error of $\delta = O\left(\Delta p^3\right)$, may not suffice. The minimization procedure suggested in Section 2.3 completely cancels the error in the subspace spanned by the "previous" solutions, and therefore does lead to an acceptable convergence.

Finally, it should be mentioned that in these examples we have assumed that $\Delta << 1$. This suggests a restriction on the step size Δp. Numerical experimentation has shown that, for each problem, there appears to be a critical step size Δp beyond which the extrapolation procedure is no longer effective. One possible explanation can be derived from the second example, by assuming that the parameter Δ is governed by the space discretization and that δ depends on Δp.

4. Step Size and Stop Criterion

To illustrate the behavior of the CG-extrapolation procedure in more detail we need to consider an actual problem. We return to the object for which the effectiveness of the method was demonstrated first, i.e., a straight thin-wire segment. The wire has length L, a circular cross section with radius a, and is embedded in a homogeneous, lossy dielectric with permittivity ε and permeability μ. The wire is excited by a delta-gap source with amplitude $V(s)$ at $z = z_g$ or by an incident electric field $\mathbf{E^i}(\mathbf{r}, s)$.

The total current $I(z, s)$ that propagates along the wire is described by Hallén's version of the thin-wire integral equation

$$\begin{aligned}\int_0^L \frac{\boldsymbol{exp}(-sR_a/c)}{4\pi R_a} I(z', s)\, dz' &= \frac{Y}{2}\int_0^L \boldsymbol{exp}\left(-s\frac{|z-z'|}{c}\right) E_z^i(z'\mathbf{u}_z, s)\, dz' + \frac{Y}{2}\boldsymbol{exp}\left(-s\frac{|z-z_g|}{c}\right) \\ &\quad + F_0(s)\,\boldsymbol{exp}\left(-s\frac{z}{c}\right) + F_L(s)\,\boldsymbol{exp}\left(-s\frac{L-z}{c}\right)\end{aligned} \tag{22}$$

In (22), we have $R_a = \sqrt{(z-z')^2 + a^2}$, while $c = 1/\sqrt{\varepsilon\mu}$ and $Y = \sqrt{\varepsilon/\mu}$ denote the complex wave speed and wave impedance of the dielectric medium, respectively. The terms proportional to $F_0(s)$ and $F_L(s)$ on the right-hand side are homogeneous solutions of the one-dimensional wave equation that can be resolved by imposing the boundary condition

$$I(0, s) = I(L, s) = 0. \tag{23}$$

In the space discretization, the Laplace transform of the *attenuated* current $\exp(-sR_a/c)\, I(z', s)$ in the left-hand side is approximated by a piecewise linear expansion and the result is integrated analytically over z'. The integral on the right-hand side is evaluated with the aid of a repeated trapezoidal rule. The resulting discretized equation assumes the form

$$\begin{aligned}\sum_{m'=1}^{M-1} W_{m-m'}\boldsymbol{exp}\left(-s\tfrac{R_{m-m'}}{c}\right) I_{m'}(s) &= \tfrac{Y}{2}\sum_{m'=0}^{M} w_{m'}\boldsymbol{exp}\left(-s\tfrac{|z_m-z_{m'}|}{c}\right)E_z^i(z_{m'}\mathbf{u}_z,s)\\ &+\tfrac{Y}{2}\boldsymbol{exp}\left(s\tfrac{|z_{m'}-z_g|}{c}\right)V(s)\\ &+F_0(s)\,\boldsymbol{exp}\left(-s\tfrac{z_m}{c}\right)+F_L(s)\,\boldsymbol{exp}\left(-s\tfrac{L-z_m}{c}\right)\end{aligned} \tag{24}$$

where $R_m = \sqrt{m^2\Delta z^2 + a^2}$, and where closed-form expressions are available for the weighting coefficients W_m and w_m.

The system of equations (24) is solved repeatedly for $s_m = \beta - im\Delta\omega$ with $\beta \geq 0$ and m = 0,1, ..., M. Subsequently, we determine the spectral inversion integral in the inverse transformation

$$I(z,t) = \frac{\exp(\beta t)}{\pi} Re \int_0^\infty I(z,\beta - i\omega)\exp(-i\omega t)\,d\omega \tag{25}$$

with the aid of a repeated trapezoidal rule and an FFT.

To demonstrate the behavior of the step size and the error criterion, we consider a wire of length L = 1 m and a = 2 mm in the frequency range from zero to 3.2 GHz with plane wave excitation at normal incidence. First we take a frequency step $\Delta\omega/2\pi$ =20 MHz, $\beta L/c_0 = 10^{-12}$ and a relative error for the CG algorithm of 10^{-8}. Figure 1 shows the number of iterations needed when we take a zero initial estimate (gray line) and three previous results (black line).

The number of iterations per frequency can be reduced by allowing for a larger relative error in the CGFFT method. The number of iterations for the same configuration with a relative error of 10^{-3} is given in Figure 2. The effect is that for both cases the number of iterations is reduced. Furthermore, the extrapolation procedure becomes also more effective. A second way to improve the efficiency of the extrapolation scheme per step is to reduce the frequency step. This is presented in Figure 3 for a frequency step of 5 MHz, $\beta L/c_0 = 10^{-12}$ and a relative error of 10^{-3}. From this figure, we observe that the highest peaks are lowered and that the average number of iterations per step is reduced. However, due to the decrease in step size, the number of frequencies for which we have to compute the current increases by a factor of four.

A third parameter that can be used to improve the efficiency of the extrapolation strategy is the parameter β. In constructing our initial estimate, we assumed that the solution to the system of equations depends in well-behaved manner on the parameter of interest. However, in case of resonance, this is no longer true. By choosing $\beta L/c_0$ very small, we may be close to a pole in the complex s-plane, i.e. close to a resonance. Therefore, we expect an improvement of the convergence of our algorithm when $\beta L/c_0$ is increased. This is shown in Figures 4 and 5 for $\beta L/c_0$ =1 and $\beta L/c_0$ =10. We see that the number of iterations per frequency step indeed decreases for increasing β. On the other hand, if we take a large value for $\beta L/c_0$, e.g. 10, the computed time-domain result is useless. This is caused by the effect that, especially for large values of t, the factor of $\exp(\beta t)$ in (25) amplifies the errors in the sampled time signal that results from the discrete Fourier transformation.

5. Physical Parameters

The scheme outlined in Section 2 has already been applied for a range of physical parameters. In Sections 6 and 7, explicit examples will be presented. In the present section, we first give a brief overview of the other

results that have been obtained until now. Most of these results have been published by now. However, a few cases remain for which we are not yet able to provide a reference. We distinguish the applications according to the physical parameter that is being varied.

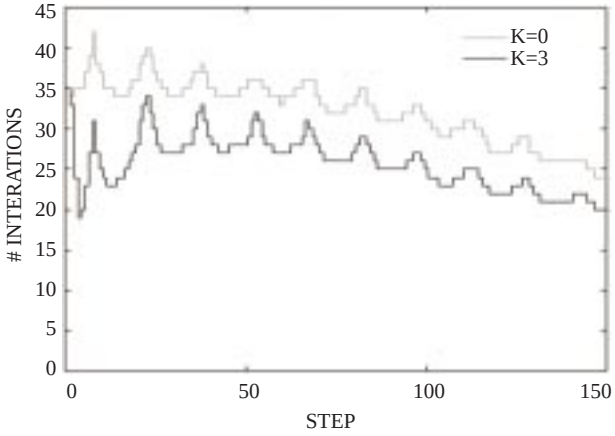

Figure 1. Number of iterations required to reach a relative error of 10^{-8} versus step for the marching-on-in-frequency version of the CGFFT method. The results were obtained for a thin wire with plane-wave excitation at normal incidence with parameters $L = 1$ m, $a = 2$ mm, $\beta L/c_0 = 10^{-12}$ and $\Delta\omega/2\pi = 20$ MHz.

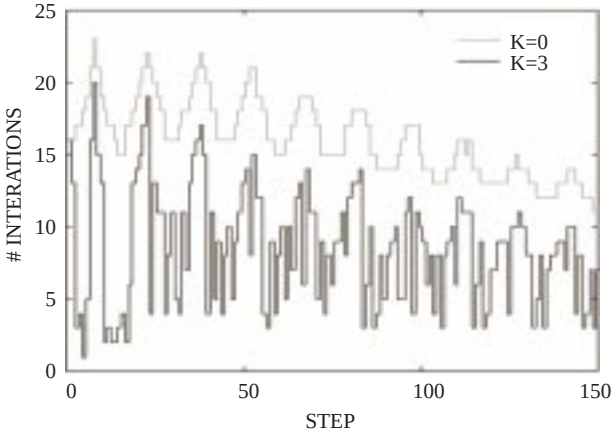

Figure 2. Number of iterations required to reach a relative error of 10^{-3} versus step for the marching-on-in-frequency version of the CGFFT method. The results were obtained for a thin wire with plane-wave excitation at normal incidence with parameters $L = 1$ m, $a = 2$ mm, $\beta L/c_0 = 10^{-12}$ and $\Delta\omega/2\pi = 20$ MHz

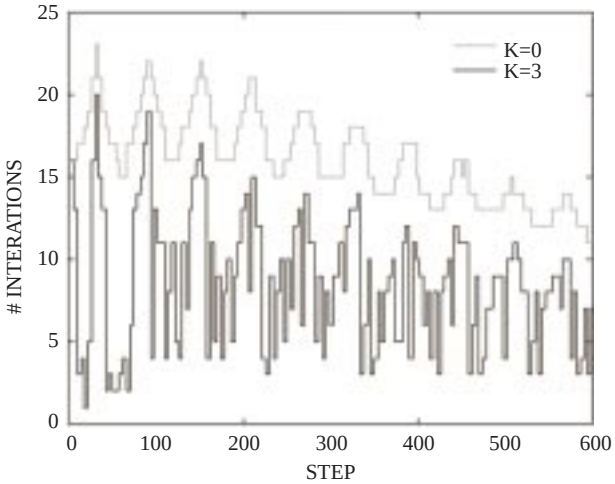

Figure 3. Number of iterations required to reach a relative error of 10^{-3} versus step for the marching-on-in-frequency version of the CGFFT method. The results were obtained for a thin wire with plane-wave excitation at normal incidence with parameters $L = 1$ m, $a = 2$ mm, $\beta L/c_0 = 10^{-12}$ and $\Delta\omega/2\pi = 5$ MHz

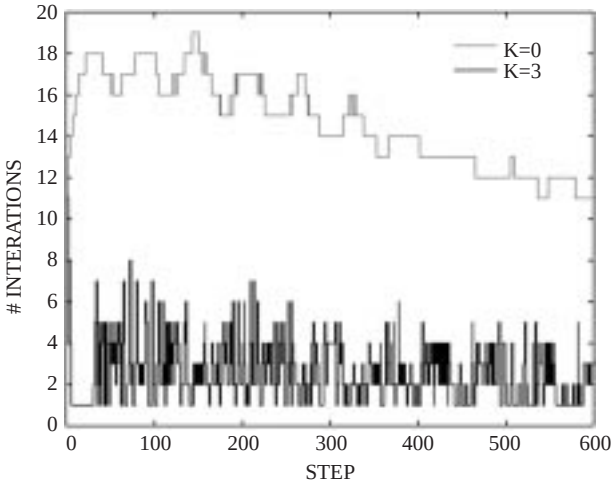

Figure 4. Number of iterations required to reach a relative error of 10^{-3} versus step for the marching-on-in-frequency version of the CGFFT method. The results were obtained for a thin wire with plane-wave excitation at normal incidence with parameters $L = 1$ m, $a = 2$ mm, $\beta L/c_0 = 1$ and $\Delta\omega/2\pi = 5$ MHz

5.1. Marching on in frequency

The approach was originally conceived as an alternative for marching-on-in-time computations, and has therefore been called "marching on in frequency". Compared with time-marching computations, the main advantage is that using results for "previous" frequencies accelerates the computations, but does not influence the final result. Therefore, the error accumulation that is inherent in time-domain schemes, and the resulting

stability problems, are implicitly avoided. Compared with conventional frequency-domain techniques, the main advantage is that the space discretization is fixed for all frequencies. Therefore, the computational effort does not increase for increasing frequencies. An additional advantage is that dispersive configurations can be handled with the same computational efficiency as their lossless counterparts.

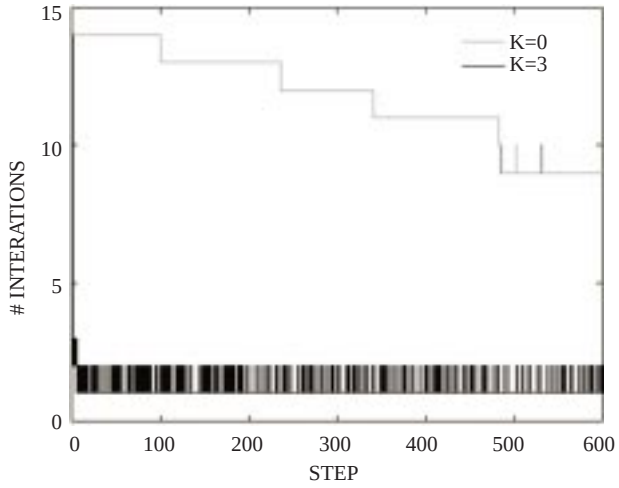

Figure 5. Number of iterations required to reach a relative error of 10^{-3} versus step for the marching-on-in-frequency version of the CGFFT method. The results were obtained for a thin wire with plane-wave excitation at normal incidence with parameters $L = 1$ m, $a = 2$ mm, $\beta L/c_0 = 10$ and $\Delta\omega/2\pi = 5$ MHz

The first example was a *thin wire* in a homogeneous background medium, for which both the Pocklington and Hallén integral equations were solved in [10] and [11]. In particular, [10] contains convergence results as well as time signals for a wire in a lossless and lossy dielectric. The extension to one and two wires near an interface between *two dielectric half-spaces* was described in [13] and [14]. The new element in this implementation was the approximation of the spatial Fourier inversion integrals by a frequency-independent combination of Gaussian quadrature rules. The justification of this approximation can be found in [15].

In [11], the approach was also applied to a two-dimensional open or closed *conducting screen*. For this configuration, a standard MoM discretization of the electric-field integral equation was used. Finally, in [12] the procedure was applied to the transient scattering by a two-dimensionally inhomogeneous, lossy *dielectric cylinder*. Here, the highlight was the space discretization. On the one hand, this discretization preserves the convolution structure of the continuous contrast-source integral equation, so that the matrix-vector products in (4) and (13) can be evaluated with the aid of two-dimensional FFT operations. On the other hand, the discretization is second-order accurate in terms of the spatial mesh size. In both [11] and [12] the excitation was restricted to electrically polarized waves.

5.2. Marching on in angle

In various applications it may be necessary to obtain the electromagnetic plane-wave response of an object for a large number of directions of incidence. When such a computation is needed at a single frequency, we can again choose a fixed space discretization. In fact, the operator products required in the minimization procedure for the initial guess are now already available from carrying out the iterative procedure at "previous" angles. The first application was the determination of the radar cross section of the *perfectly*

conducting screen described in [10], which was carried out directly after that paper was submitted. Here, the incident field was an electrically polarized incident plane wave.

The second application originates from the solution of the inverse-profiling problem of a two-dimensionally inhomogeneous, *lossy dielectric cylinder* in a homogeneous surrounding medium [16]. The cylinder is excited by an electrically polarized plane wave with a varying direction of incidence or an electric line source on a circular contour that surrounds the cylinder. The aim of the computation is to determine the complex permittivity from scattered-field values at a single frequency. In each step of the reconstruction procedure, we first determine the field that would be present in the configuration as it was estimated in the previous step. Subsequently, we update the unknown permittivity by minimizing a cost function involving the difference between the simulated and known scattered fields. In the first few steps of the reconstruction, the approximate fields are computed by marching on in angle. Once the inversion begins to converge, it is more efficient to march in contrast.

In both cases, it turns out that the full scattering operator of a two-dimensional object can be obtained with a computational effort that is comparable to solving a few direct-scattering problems "from scratch".

5.3. Marching on in shape

In the design of antennas or microstrip circuits, it may be necessary to "tune" the dimensions of one or more of the elements of the structure. This can be achieved by varying the length of the element in that particular direction. Again, we keep the size of the matrix fixed. This may result in too fine a discretization when that length is shorter than the desired maximum. However, the extra computational effort is more than compensated for by the reduction in computation time due to the use of the extrapolation procedure.

The first and most simple example is the computation of the current along a *wire antenna* of varying length. Changing the length over a fixed range may allow us to select the best resonance at a given frequency. This application was demonstrated successfully for the thin-wire code described in [10,11]. Results of a similar computation for a *flat rectangular plate* will be presented in Section 6.1.

A similar situation arises when the shape of a homogeneous object of known constitution needs to be reconstructed or changes gradually in time. The so-called level-set algorithm described in [17] models the reconstruction process of a two-dimensional, homogeneous dielectric cylinder with known permittivity as the evolution of a gradually varying boundary contour. To test the efficiency of our modeling approach, the forward field computation of the algorithm described in [17] was replaced by the forward scheme proposed in [12]. In this scheme, the boundary and the contrast are treated separately, so that a continuously changing boundary corresponds to a continuous change in a set of weighting coefficients of a fixed dimension. Even though the forward scheme described in [12] is based on a domain integral equation, a considerable reduction was obtained in the computation time for a complete reconstruction.

In this category, the ultimate challenge is the computation of the field scattered by a mechanically vibrating, three-dimensional conducting object. This case remains to be implemented.

5.4. Marching on in search direction

The most advanced application until now concerns the combination of our forward modeling strategy with nonlinear optimization. Until now, we have only dealt with the inverse-profiling problem for a two-dimensionally inhomogeneous, lossy dielectric cylinder discussed in [16]. As mentioned above, for this configuration the full scattering operator can be determined at the cost of a few individual field computations.

The availability of the scattering matrix offers the possibility to overcome some of the limitations of linearized schemes. The idea is to replace the determination of the profile update in a linearized scheme by a line search in a nonlinear optimization scheme. We search in the so-called gradient direction, which can be determined from the scattered field. There is no need of inverting matrices or solving adjoint problems; only straightforward integrations are involved. Until now, the expression for the gradient direction has hardly been used in practice, because it was too time consuming to compute the full scattering matrix with conventional solution methods. With the fast forward scheme described in this paper, that is no longer a problem. As described in Section 5.3, we march on in angle in the first two steps of each line search. In subsequent steps, however, marching in search direction is considerably more efficient. This advantage shows up especially near convergence of the search algorithm, where the field in the estimated configuration is almost constant.

The major attraction of the procedure proposed above is that it allows us to solve a nonlinear optimization problem for a geometry that is characterized by a number of configuration parameters, while preserving the variation in only a single search parameter.

6. Scattering by Three-Dimensional Objects

To illustrate our approach, we have extended existing implementations of the CGFFT procedure for two three-dimensional objects that have become standards in the literature. In both cases, no special precautions were taken to enhance the discretization, which is first-order accurate as a function of the mesh size.

6.1. Scattering by a flat plate

The first example is a flat, rectangular plate in free space located at $0 < x < a, \quad 0 < y < b$ and $z = 0$ [18]. For this problem, we solve the well-known electric-field integral equation

$$\left[\nabla_T \nabla_T . + \frac{s}{c_0^2}\right] \int_0^a dx' \int_0^b dy' \frac{\boldsymbol{exp}\left(-sR/c_0\right)}{4\pi R} \boldsymbol{J}_S\left(\boldsymbol{r}'_T, s\right) = -s\varepsilon_0 \boldsymbol{E}_T^i\left(\boldsymbol{r}_T, s\right), \tag{26}$$

where s is a complex frequency, $R = |\boldsymbol{r}_T - \boldsymbol{r}'_T|$, and where the subscript $_T$ stands for a transverse component. The unknown surface current $\boldsymbol{J}_S\left(\boldsymbol{r}_T, s\right)$ is approximated by rooftop functions, and we use a weak formulation of (26), weighted by the same rooftop functions. In the resulting discretized form, the convolution symmetry is preserved, so that the matrix-vector products in the conjugate-gradient procedure can be evaluated with the aid of two-dimensional FFT operations.

In particular, we have computed the monostatic radar cross section of $\lambda \times \lambda$ plate for the special case $s = -i\omega$. A plane wave is incident on the plate at an angle θ with respect to the z-axis and an angle $\phi = 90^\circ$ with respect to the x-axis. The incident plane wave is x-polarized. The discretized plate has a mesh of $3\mathrm{l} \times 3\mathrm{l}$ points. Figure 6 shows the number of iterations for increasing θ. The gray line represents starting from a zero initial estimate, and the black line is for two previous results in the initial estimate, i.e. $K = 2$. Figure 7 presents the monostatic radar cross section of the $\lambda \times \lambda$ plate in the plane $\phi = 90^\circ$.

The last result for the plate concerns marching on in length. The idea was inspired by the shape sensitivity analysis in [l9,20]. Here, we start from a $\lambda \times \lambda$ plate and we increase the length of the plate in 100 steps to a $2\lambda \times \lambda$ plate. We used a fixed spatial discretization of $62 \times 3\mathrm{l}$ mesh points. The number of

iterations required to reach a relative error of 10^{-3} versus the length of the plate is shown in Figure 8. In the computations leading to Figures 6 and 8, it turned out that extrapolation with $K = 2$ was in fact more efficient than extrapolation with $K = 3$.

6.2. Scattering by an inhomogeneous dielectric cube

The second example is an inhomogeneous dielectric cube, again in free space. We formulate the scattering problem as a domain integral equation over the object domain D as

$$\mathbf{E}^i(r,s) = \frac{\mathbf{D}(\mathbf{r},s)}{\varepsilon(\mathbf{r},s)} + \left(\frac{s^2}{c_0} - \nabla\nabla.\right)\mathbf{A}(\mathbf{r},s) \tag{27}$$

where s is a complex frequency and where the vector potential $\mathbf{A}(\mathbf{r},s)$ is given by

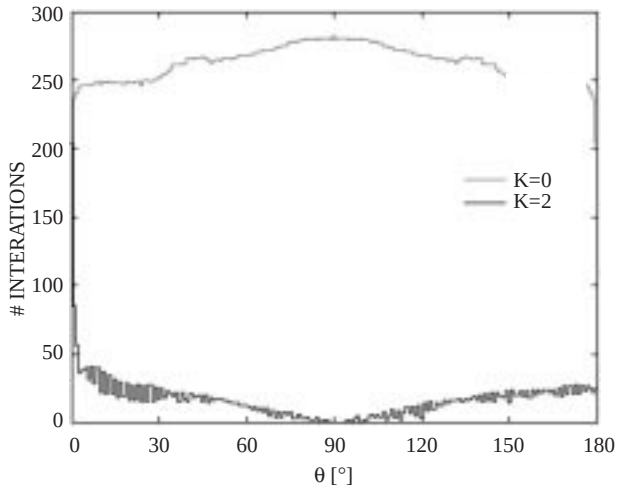

Figure 6. Number of iterations required to reach a relative error of 10^{-3} versus angle of incidence for the marching-on-in-angle version of the CGFFT method for a flat plate using zero (gray line) and two previous results (black line) as an initial estimate

$$\mathbf{A}(\mathbf{r},s) = \frac{1}{\varepsilon_0}\iiint_D \frac{\boldsymbol{exp}(-sR/c_0)}{4\pi R}\frac{\varepsilon(\mathbf{r},s)-\varepsilon_0}{\varepsilon(\mathbf{r},s)}\mathbf{D}(\mathbf{r},s)dV', \tag{28}$$

where $R = |\mathbf{r} - \mathbf{r}'|$. We take the contrast function in (28) constant in each rectangular subdomain in the space discretization. Like the current in the plate problem, the dielectric displacement $\mathbf{D}(\mathbf{r},s)$ is approximated by an expansion that is piecewise linear in the longitudinal direction and constant in the transverse directions. The Green's function is replaced by a weak form, and the result is weighted by testing functions that are identical to the expansion functions. Again, the space discretization preserves the convolution symmetry of the continuous form of the integral equation given in (27) and (28). More details can be found in [21] and [22].

As an illustration, we have modeled a cube of muscle tissue centered inside a cube of fat tissue. The incident field is x-polarized with propagation vector parallel to the z-axis and a strength of 1 V/m. The dispersive tissues are modeled using a Debye model [23] and the dimensions of the inner and outer cubes are

0.14 m and 0.30 m, respectively. The discretized object has $30 \times 30 \times 30$ mesh points. The field is computed in the middle of the muscle cube for real-valued frequencies $s = -i\omega = -i2\pi f$ of 100 to 600 MHz and then converted to a time domain signal. The number of iterations needed is shown in Figure 9, where the gray line is for a zero initial estimate, and the black line for minimization using two previous results. Again, using $K = 2$ in the extrapolation procedure led to the most rapid convergence. The time signal, shown in Figure 10, is computed by an FFT using the waveform $\boldsymbol{exp}\left[-\frac{(t-\tau)^2}{2T^2}\right] Sin\left(\omega_0 t\right)$, where $\tau = 14$ ns, $T = 2.75$ ns and $\omega_0/2\pi = 450$ MHz.

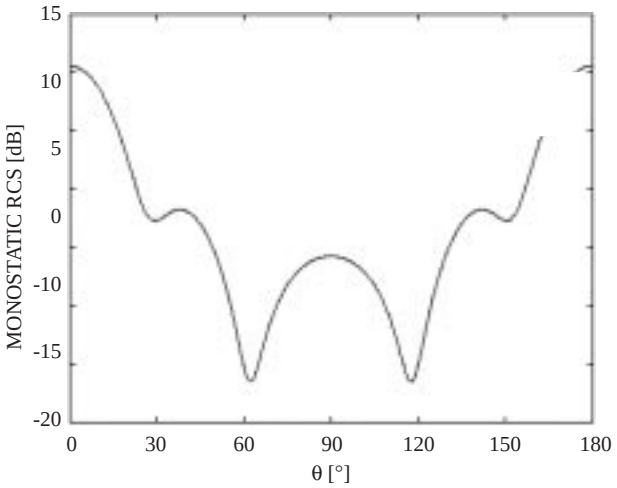

Figure 7. Monostatic radar cross section versus angle of incidence for a $\lambda \times \lambda$ plate.

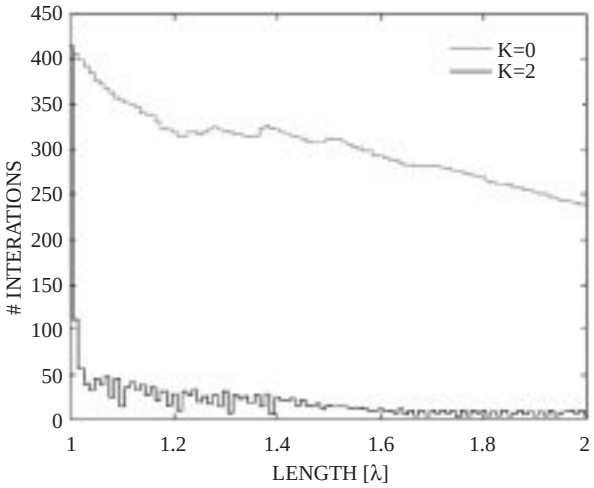

Figure 8. Number of iterations required to reach a relative error of 10^{-3} versus length of the plate for the marching-on-in-length version of the CGFFT method for a flat plate using zero (gray line) and two previous results (black line) as an initial estimate.

7. Objects in a Complex Environment

Finally, we discuss two examples where the medium that surrounds the scattering object is no longer homogeneous. Even for such an environment, a Green's function can be defined as an appropriately normalized response to an elementary source. However, the convolution structure that determines to a considerable extent the efficiency of the conjugate-gradient method is only preserved if the surrounding medium has translation symmetry in the same directions as the scattering object. In that case, we can adapt the Green 's function in the integral equation. Otherwise, partitioning the configuration may be the only solution.

7.1. Two wire antennas over a layered half-space

In the first example, the Green 's function can be generalized. The configuration consists of two resistively loaded wires parallel to a plane-stratified inhomogeneous dielectric layer on top of a homogeneous, lossy half-space. An impression is given in Figure 11. This example is a continuation of the research described in [13,14], which is aimed at designing a simple antenna system that is capable of detecting properties of the subsurface. In this particular configuration, we aim at visualizing the constitutive properties of the dielectric slab.

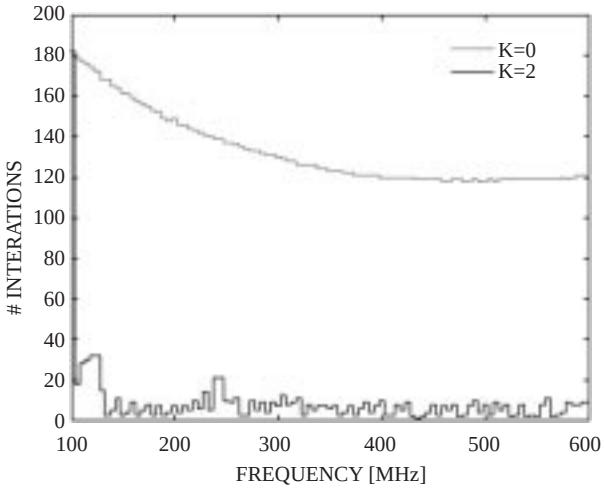

Figure 9. Number of iterations required to reach a relative error of 10^{-3} versus frequency for the marching-on-in-frequency version of the CGFFT method for an inhomogeneous dielectric cube using zero (gray line) and two previous results (black line) as an initial estimate

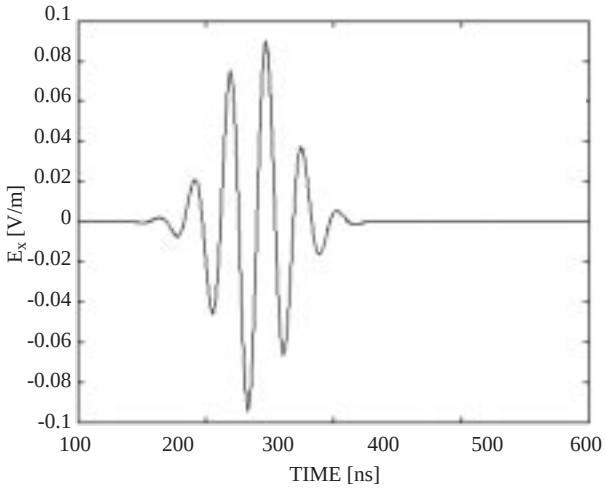

Figure 10. Time domain signal at the center of the muscle cube for an incident x-polarized wave of 1 V/m

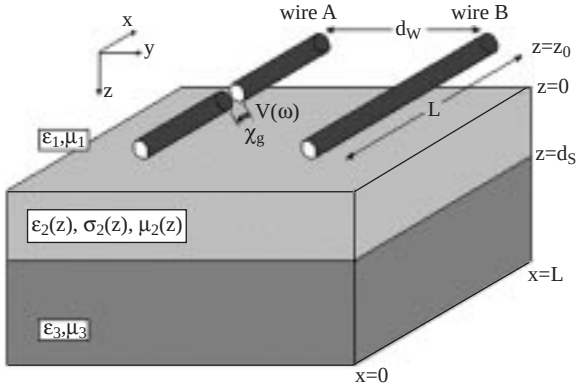

Figure 11. Two coated wire antennas over a layered dielectric half space.

For the current along Wire A, we obtain the Pocklington-type integral equation

$$\left[\partial_x^2 - \frac{s^2}{c_1^2}\right] \int_0^L \frac{\boldsymbol{exp}(-sR_a/c_1)}{4\pi R_a} I^A(x', s)\, dx' - s\varepsilon_1 R^L(x)\, I^A(x, s) = \\ -s\varepsilon_1 V_A(s)\, \delta(x - x_g) - s\varepsilon_1 E_x^i(\mathbf{r}_A, s) \tag{29}$$

where the notation is in analogy with (22). The only new element is the resistance profile $R^L(x)$. The incident field on Wire A is in fact a secondary field caused by the induced current along Wire B and reflections at the interface. In particular, we have

$$
\begin{aligned}
s\varepsilon_1 E_x^i(\mathbf{r}_A, s) &= \left[\partial_x^2 - \tfrac{s^2}{c_1^2}\right] \int_0^L \frac{\boldsymbol{exp}(-sR_d/c_1)}{4\pi R_d} I^B(x', s)\, dx' \\
&+ s\varepsilon_1 \int_0^L G_x^r(x - x', 0, z_0, s)\, I^A(x', s)\, dx' \\
&+ s\varepsilon_1 \int_0^L G_x^r(x - x', -d_W, z_0, s)\, I^B(x', s)\, dx'
\end{aligned} \tag{30}
$$

where $R_d = \sqrt{(x - x')^2 + d_W^2}$ and $G_x^r(x, y, z, s)$ is the x-component of the electric field that would be obtained by exciting the stratified configuration with a horizontal dipole in the x-direction located at $x = y = 0$ and $z = z_0$. The first term on the right-hand side of (30) represents the field directly radiated by the currents along Wire B, and the next two terms represent the reflected fields due to the currents along Wire A and B, respectively.

The solution of the integral equation given in (29) and (30) proceeds in the same way as described in [14]. First, an equivalent Hallén equation is derived. Next, symmetry is invoked to break up the computation into the determination of the "even" and "odd" solutions $I^{\pm}(x, s) = \frac{1}{2}\left[I^A(x, s) \pm I^B(x, s)\right]$. Finally, the problem is discretized in space in a similar manner as the equation for the single wire discussed in Section 4. The fact that the integrals (29) and (30) still have the form of a convolution is exploited to apply the CGFFT method. The computational effort is consumed mainly in the evaluation of the Green's functions $G_x^r(x, 0, z_0, s)$ and $G_x^r(x, d_W, z_0, s)$. We use a combination of Gaussian quadrature rules to evaluate the spectral integral, and a one-dimensional contrast-source integral equation to determine the spectral constituents. In both cases, the discretization is independent of the frequency [15].

A representative result is shown in Figure 12, where we consider the transient current on Wire B for three different permittivity profiles in the dielectric layer. This figure shows that, for a proper choice of the resistance $R^L(x)$, the transient current has an almost local correspondence to the permittivity $\varepsilon(z)$. In fact, time signals like the ones shown in Figure 12 can be combined into an "electromagnetic seismogram" similar to the ones used in geophysics. More details will be published in [24].

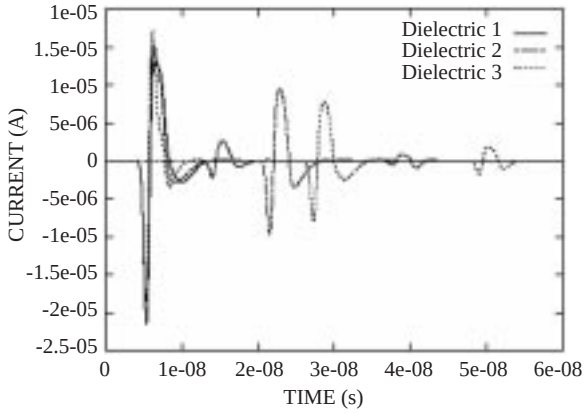

Figure 12. Current at the center of wire B versus time. The wires are loaded with a Wu-King profile and excited by a Gaussian pulse. Configuration parameters: $L = 1$ m, $a = 2$ mm, $d_w = 1$ m, $z_0 = -0.25$ m and $d_S = 1$ m. Solid line: $\varepsilon_{2r} = 2$ (Dielectric 1). Broken line: $\varepsilon_{2r}(z) = 2 + 9z$ (Dielectric 2). Dotted line: $\varepsilon_{2r} = 11$ (Dielectric 3). $\mu_{2r} = 1$ in all cases

7.2. Dielectric cylinder inside a metal container

The last example is a configuration where the exterior medium is not symmetric in the coordinates along which the convolution is carried out. We consider an inhomogeneous, lossy dielectric cylinder in an observation domain D_O, embedded in a water-filled perfectly conducting circular container. The configuration is excited by a time-harmonic electric line source on a circular contour ∂D_O outside the cylinder. A cross section of the configuration is displayed in Figure 13. The electric field strength must be computed on the observation contour ∂D_O as well as in the observation domain D_O. This configuration was inspired by a scanner that is presently under construction at CNRS/Supélec, Gif-sur-Yvette, Paris, France [25]. The aim of our research is to generalize the linear and nonlinear inversion schemes for a dielectric cylinder in a homogeneous medium as outlined in [16] to the geometry shown in Figure 13.

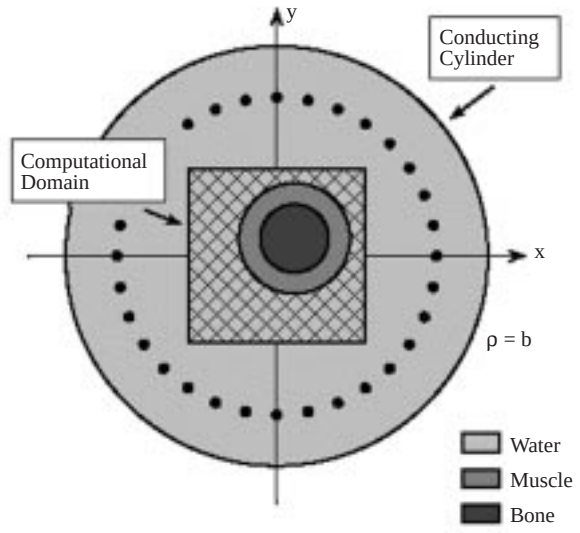

Figure 13. Model for a human arm inside a water-filled perfectly conducting circular container. The shaded region is the domain in which the field is computed numerically

As described in Sections 5.2 and 5.4, a key element in the schemes described in [16] is the fast computation of the fields that would be present in an estimated configuration. In particular, we consider *Green's function*, i.e., the solution of the second-order differential equation

$$\left[\nabla_T^2 - s^2 \varepsilon_r(\boldsymbol{\rho})\right] G(\boldsymbol{\rho}, \boldsymbol{\rho}_S) = -\delta(\boldsymbol{\rho} - \boldsymbol{\rho}_S) \tag{31}$$

that satisfies the proper conditions outside ∂D_O. For the homogeneous medium, $G_{hom}(\boldsymbol{\rho}, \boldsymbol{\rho}_S)$ satisfies the radiation condition as $\rho \rightarrow \infty$. For the cylinder in the container, we have $G_{cyl}(\boldsymbol{\rho}, \boldsymbol{\rho}_S) = 0$ at $\rho = b$.

For a homogeneous environment, the field computation is based on the contrast-source integral equation

$$G_{hom}(\boldsymbol{\rho}, \boldsymbol{\rho}_S) = \frac{1}{2\pi} K_0\left(\frac{s|\boldsymbol{\rho} - \boldsymbol{\rho}_S|}{c_1}\right) - \frac{s^2}{2\pi c_0^2} \iint_{D_O} K_0\left(\frac{s|\boldsymbol{\rho} - \boldsymbol{\rho}'|}{c_1}\right) [\varepsilon_r(\boldsymbol{\rho}') - \varepsilon_{1r}] G_{hom}(\boldsymbol{\rho}', \boldsymbol{\rho}_S)\, dA(\boldsymbol{\rho}'), \tag{32}$$

where K_0 denotes the modified Bessel function of the first kind of order zero and where the frequency dependence has not been indicated explicitly. The space discretization of the integrals in (32) is based on approximating suitable parts of the integrands by piecewise-bilinear approximations on a rectangular mesh, and integrating analytically over square subregions. The resulting discretized form is second-order accurate in the mesh size and preserves the convolution symmetry. Thus, the CGFFT method remains applicable. More details can be found in [12].

For the cylinder in the actual environment, we express the field in the vicinity of ∂D_O in terms of an angular spectral representation

$$\begin{aligned} G_{cyl}(\boldsymbol{\rho}, \boldsymbol{\rho}_S) &= \tfrac{1}{2\pi} \sum_{m=-\infty}^{\infty} \boldsymbol{exp}[im(\varphi - \varphi_S)] I_m\left(\tfrac{s\rho_<}{c_1}\right) K_m\left(\tfrac{s\rho_>}{c_1}\right) \\ &+ \sum_{m=-\infty}^{\infty} \boldsymbol{exp}(im\varphi)\, C_m I_m\left(\tfrac{s\rho}{c_1}\right) + \sum_{m=-\infty}^{\infty} \boldsymbol{exp}(im\varphi)\, D_m K_m\left(\tfrac{s\rho}{c_1}\right). \end{aligned} \tag{33}$$

In the right-hand side of (33), the first term can be identified as direct radiation from the line source, the second term as a source-free field due to reflections at the casing, and the third term as a scattered field originating from the dielectric cylinder. Using the linearity of the problem, we introduce a reflection coefficient for the empty casing and a scattering operator for the dielectric cylinder in a homogeneous environment. With the aid of these operators, we then derive a linear equation for the coefficients $\{C_m\}$:

$$\begin{aligned} C_m - R_m \sum_{m'=-\infty}^{\infty} S_{m,m'} C_{m'} &= \tfrac{1}{2\pi} R_m \boldsymbol{exp}(-im\varphi_S)\, I_m\left(\tfrac{s\rho_O}{c_1}\right) \\ &+ \tfrac{1}{2\pi} R_m \sum_{m'=-\infty}^{\infty} S_{m,m'} \boldsymbol{exp}(-im'\varphi_S)\, K_{m'}\left(\tfrac{s\rho_O}{c_1}\right) \end{aligned} \tag{34}$$

This ,equation is solved by truncating the summations over m', and inverting the resulting matrix equation. The coefficients $\{D_m\}$ are then obtained from the definition of the reflection coefficient:

$$D_m = R_m \left[\frac{1}{2\pi} \exp(-im\varphi_S)\, K_m\left(\frac{s\rho_O}{c_1}\right) + C_m \right]. \tag{35}$$

Finally, the field in the observation domain D_O is obtained by constructing an equivalent surface current in a homogeneous background. For $\rho < b$, this current generates the source-free field represented by the second term on the right-hand side of (33). Using the uniqueness of the solution of the homogeneous wave equation then leads to the conclusion that the total field in D_O is given by the corresponding superposition of total fields

$$G_{cyl}(\boldsymbol{\rho}, \boldsymbol{\rho}_S) = G_{hom}(\boldsymbol{\rho}, \boldsymbol{\rho}_s) + \int_0^{2\pi} W(\varphi_P, \varphi_S)\, G_{hom}(\boldsymbol{\rho}, \boldsymbol{\rho}_P)\, d\varphi_P, \tag{36}$$

where the weighting function $W(\varphi_P, \varphi_S)$ is related to the coefficients $\{C_m\}$ by an angular Fourier transformation.

As an illustration, we consider in Figure (14) the case of two homogeneous circular cylinders embedded in water. The permittivity of both cylinders is representative of muscle. Figure 14a corresponds to a homogeneous environment and Figure 14b to the presence of a conducting cylinder. More details have already been published in a workshop presentation [26]; a full paper is in preparation.

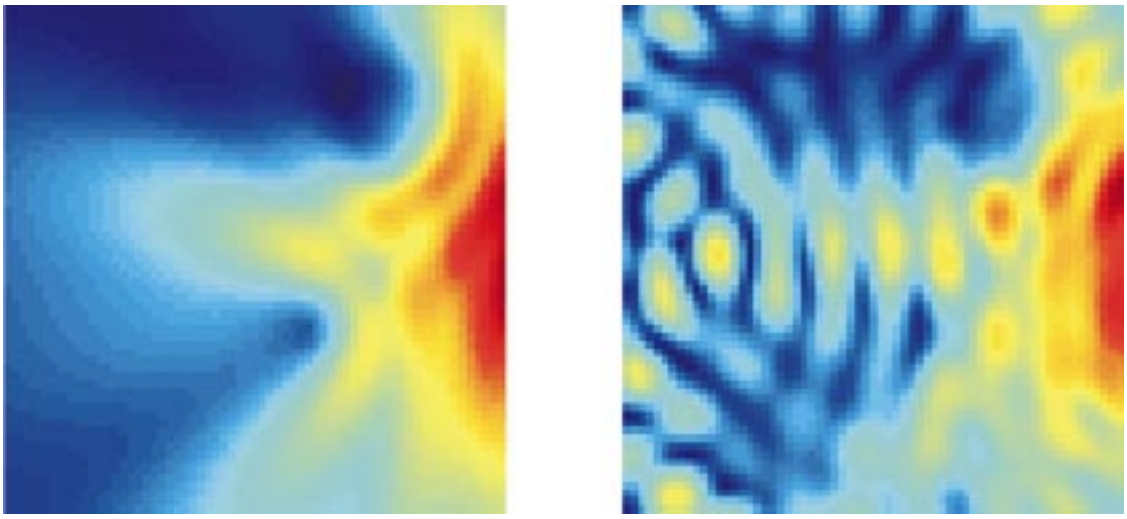

(a) (b)

Figure 14. Fields for two circular dielectric cylinders with $\varepsilon_{r,m} = 54.2 + i38.4$ embedded in water with $\varepsilon_{r,W} = 76.3 + i3.9$ at $f = 434$ MHz. (a): homogeneous environment; (b): cylindrical casing. The line source is located to the right of the computational domain.

8. Conclusions

In this paper, we have extended the conventional conjugate-gradient method with a dedicated extrapolation procedure that considerably enhances the speed of convergence. Unfortunately, a rigorous analysis of the effectiveness of the combined procedure is not available. However, extensive numerical experimentation has at least given us an idea of what is going on. In this paper, we have illustrated this for two simple three-by-three systems. Further, the role of the step size and the stop criterion has been discussed for the simple case of the thin wire. Although the procedure has already been demonstrated successfully for a range of applications, including transient scattering, RCS computations and inverse profiling, until now no applications to three-dimensional configurations have been reported. In the present paper, this gap has been filled. Finally, we have discussed two applications for an object in a more general environment.

It is the authors' experience that several ideas that were presented in this paper at first appear to be counter-intuitive. For example, the concept of marching on in frequency requires the use of a frequency-independent space discretization. Although such a discretization is used in any FDTD computation, frequency-domain algorithms tend to use a fixed number of points per wavelength. Abandoning this choice allows us to avoid the stability problems that are inherent in time-marching computations, and to extend our approach to configurations where both the scattering object and the surrounding medium may be dispersive. A second example is the observation that the computational cost of determining the full scattering matrix of an object in a homogeneous environment is comparable to the cost of solving a few individual field problems "from scratch". This observation is the basis of our nonlinear approach to inverse

scattering as well as the embedding approach for handling the dielectric cylinder in a water-filled metal container.

Finally, the ideas presented in this paper open up the possibility of handling applications that, until now, were not considered to be in the range of computational electromagnetics. For example, we are presently investigating the optimization of an infinite antenna array that can be described by a limited number of physical parameters. A possible application of the embedding approach is the computation of electromagnetic fields in infinite and large, finite periodic structures like frequency-selective surfaces and electromagnetic-bandgap materials.

Acknowledgements

The authors would like to thank Prof. Amelia Rubio Bretones from the University of Granada, Spain and Dr. Ann Franchois from the University of Ghent, Belgium, for the use of joint work in Section 7. The third author would like to thank the Deputy Director and the Integrated Topside Design Program Manager, both from the TNO Physics and Electronics Laboratory, for the financial support that enabled him to participate in this research project at the Eindhoven University of Technology.

References

[1] R. F. Harrington, "Field computation by Moment Methods," New York: Macmillan, 1968.

[2] G. H. Golub and C. F. van Loan, "Matrix Computations Third Edition," Baltimore and London: The Johns Hopkins University Press, 1996.

[3] P. M. van den Berg, "Iterative computational techniques in scattering based upon the integrated square error criterion," IEEE Trans. Antennas Propagat., vol. 32, pp. 1063-1071, October 1984.

[4] P. M. van den Berg, "Iterative schemes based on the minimization of the error in field problems," Electromagnetics, vol. 5, pp. 237-262, April 1985.

[5] T. K. Sarkar, E. Arvas and S. M. Rao, "Application of the fast Fourier transform and the conjugate gradient method for the solution of electromagnetic radiation from electrically large and small conducting bodies," Electromagnetics, vol. 5, pp. 99-122, April 1985.

[6] S. A. Bokhari and N. A. Balakrishnan, "A method to extend the spectral iteration technique," IEEE Trans. Antennas Propagat., vol. 34, pp. 51-57, January 1986.

[7] T. K. Sarkar, E. Arvas and S. M. Rao, "Application of the FFT and the conjugate gradient method for the solution of electromagnetic radiation from electrically large and small conducting bodies", IEEE Trans. Antennas Propagat., vol. 34, pp. 635-640, May 1986.

[8] Yuan Zhuang, Ke-Li Wu, Chen Wu, J. Litva, "A combined full-wave CGFFT method for rigorous analysis of large microstrip antenna arrays", IEEE Trans. Antennas Propagat., vol. 44, pp. 102-109, January 1996.

[9] J. Basterrechea and M. F. Catedra, "Computatation of microstrip S-parameter using a CG-FFT scheme", IEEE Trans. Microwawe Theory Tech., vol. 42, pp. 234-240, February 1994.

[10] A. G. Tijhuis, Z. Q. Peng and A. Rubio Bretones, "'Iransient excitation of a straight thin wire segment: a new look at an old problem", IEEE Trans. Antennas Propagat., vol. 40, pp. 1132-1146, October 1992.

[11] A. G. Tijhuis and Z. Q. Peng, "Marching-on-in-fequency method for solving integral equations in transient electromagnetic scattering", lEE Proc. H, vol. 138, pp. 347-355, August 1991.

[12] Z. Q. Peng and A. G. Tijhuis, "'Iransient scattering by a lossy dielectric cylinder: marching-on-in-frequency approach", J. Electromagn. Wawes Applicat., vol. 7, pp. 739-763, July 1993.

[13] A. Rubio Bretones and A. G. Tijhuis, "Transient excitation of a straight thin wire segment over an interface between two dielectric halfspaces", Radio Sci., vol. 30, pp. 1723-1738, November-December 1995.

[14] A. Rubio Bretones and A. G. Tijhuis, "Transient excitation two coupled wires over an interface between two dielectric half spaces", Radio Sci., vol. 32, pp. 1723-1738, January-February 1997.

[15] A. G. Tijhuis and A. Rubio Bretones, "Transient excitation of a layered dielectric medium by a pulsed electric dipole", IEEE Trans Antennas Propagat., vol. 48, pp. 1673-1684, October 2000.

[16] A. G. Tijhuis, K. Belkebir, A. C. S. Litman and B.P. de Hon, "Theoretical and computational aspects of 2-D inverse profiling", IEEE Trans. Geosc. Remote Sensing, vol. 39, pp. 1316-1330, June 2001.

[17] A. Litman, D Lesselier and F. Santosa, "Reconstruction of a 2-D binary obstacle by controlled evolution of a level set", Inv. Probl., vol. 14, pp. 685-706, May-June 1998.

[18] A. P. M. Zwamborn and P. M. van den Berg, "The weak form of the conjugate gradient method for plate problems", IEEE Trans. Antennas Propagat., Vol. 39, pp. 224-228, February 1991.

[19] J. Ureel and D. De Zutter, "Shape sensitivities of capacitances of planar conducting surfaces using the method of moments", IEEE Trans. Microwawe Theory Tech., vol. 44, pp. 198-207, February 1996.

[20] J. Ureel and D. De Zutter, "A new method for obtaining shape sensitivities of planar microstrip structures by a full-wave analysis", IEEE Trans. Microwawe Theory Tech., vol. 44, pp. 249-260, February 1996.

[21] A. P. M. Zwamborn, and P. M. van den Berg, "The three-dimensional weak form of the conjugate gradient FFT method for solving scattering problems", IEEE Trans. Microwawe Theory Tech., 40,1757-1766, September 1992.

[22] A. P. M. Zwamborn, and P. M. van den Berg, "Computation of electromagnetic fields inside strongly inhomogeneous objects by the weak conjugate gradient FFT method", JOSA A, Vol. 11, pp. 1414-1421, April 1994.

[23] E. S. A. M. Lepelaars, "Electromagnetic pulse distortion in living tissue", Med. Biol. Eng. Comput., Vol. 34, 213-220, May 1996.

[24] A. Rubio Bretones, A.G. Tijhuis, R. Gomez Martin and S.H.J.A. Vossen, "Transient excitation of two loaded wires above a half-space with a cover layer", IEEE Trans. Antennas Propagat., accepted for publication.

[25] J. M. Geffrin, J. Ch. Bolomey, K. Belkebir and A. G. Tijhuis, "Reconstruction of a two-dimensional complex permittivity distribution -application to biological tissue", Proceedings of the PIERS Symposium, Cambridge, Massachusetts, U.S.A., July 7-11, 1997, p. 738.

[26] A. Tijhuis, A. Franchois, W. Janssen and P. Zwamborn, "Two-dimensional inverse profiling in a complex environment", Workshop on Microwawe Imaging Methods, Ch. Pichot and J.-Y. Dauvignac (Eds.), European Microwave Week, Paris, France, October 2-6, 2000.